6162 *Chem. Mater.* **2010,** *22,* 6162–6170
DOI:10.1021/cm102155m

CHEMISTRY OF MATERIALS
Article

In Situ X-ray Absorption Near-Edge Structure Spectroscopy of ZnO Nanowire Growth During Chemical Bath Deposition

Kevin M. McPeak,[†] Matthew A. Becker,[‡] Nathan G. Britton,[†] Hasti Majidi,[†] Bruce A. Bunker,[‡] and Jason B. Baxter*,[†]

[†]*Department of Chemical and Biological Engineering, Drexel University, Philadelphia, Pennsylvania 19104, United States , and* [‡]*Department of Physics, University of Notre Dame, Notre Dame, Indiana 46556, United States*

Received July 31, 2010. Revised Manuscript Received October 5, 2010

Chemical bath deposition (CBD) offers a simple and inexpensive route to deposit semiconductor nanostructures, but lack of fundamental understanding and control of the underlying chemistry has limited its versatility. Here we report the first use of *in situ* X-ray absorption spectroscopy during CBD, enabling detailed investigation of both reaction mechanisms and kinetics of ZnO nanowire growth from zinc nitrate and hexamethylenetetramine (HMTA) precursors. Time-resolved X-ray absorption near-edge structure (XANES) spectra were used to quantify Zn(II) speciation in both solution and solid phases. ZnO crystallizes directly from $[Zn(H_2O)_6]^{2+}$ without long-lived intermediates. Using ZnO nanowire deposition as an example, this study establishes *in situ* XANES spectroscopy as an excellent quantitative tool to understand CBD of nanomaterials.

Introduction

Chemical bath deposition (CBD) is widely used in the laboratory to deposit semiconductor nanostructures and thin films and also in industry for deposition of CdS buffer layers for thin film photovoltaics.[1] During CBD, material is deposited onto a substrate from a supersaturated solution of dilute aqueous precursors such as metal salts, complexing agents, and pH buffers. CBD has several advantages compared to vapor phase growth methods, including low cost, operation at low temperature and atmospheric pressure, and scalability to large area substrates. However, a lack of fundamental understanding of the underlying CBD chemistry has led to criticism for being a recipe-based approach. Transitioning CBD from a recipe-based approach to one with predictive control over the deposition products will enhance our ability to tailor the morphology and properties of deposited materials and will also enable novel synthesis routes for new materials. Such a transition requires a molecular-level understanding of the deposition chemistry that can only be obtained through *in situ* spectroscopy.

Here we report the first use of *in situ* X-ray absorption near-edge structure (XANES) spectroscopy to probe the deposition of nanostructures by CBD, and we show that it enables investigation of growth mechanisms and kinetics with unprecedented detail. Specifically, *in situ* XANES spectroscopy was used to probe the coordination environment of Zn(II) in real time during the CBD of ZnO nanowires from zinc nitrate and hexamethylenetetramine (HMTA) precursors. XANES spectroscopy is an element-specific probe that is highly sensitive to the local structure around the absorbing atom due to single and multiple scattering of the ejected photoelectron.[2,3] The high degree of structural sensitivity provided by XANES allows the coordination environment of metal ions to be determined quantitatively upon comparison to spectra of known standards. XANES spectroscopy does not require the sample to exhibit long-range order and can therefore be used to characterize liquid, amorphous, and crystalline materials.[2,4] Furthermore, XANES is sensitive to very low concentrations of absorber atoms due to the high photon flux of synchrotron radiation, enabling *in situ* investigation of processes including ion exchange and electrodeposition of nanomaterials.[5,6] Metal ion concentrations as low as 1 ppm (~0.01 mM for Zn(II) ions) are readily detectable at the beamline used for this work. The combination of high sensitivity to the coordination environment of the absorber atom and ability to probe

*To whom correspondence should be addressed. E-mail: jbaxter@drexel.edu.

(1) Hodes, G. *Chemical Solution Deposition of Semiconductor Films*; Marcel Dekker, Inc.: New York, 2003.
(2) Brown, G. E.; Calas, G.; Waychunas, G. A.; Petiau, J. *Rev. Miner.* **1988**, *18*, 431.
(3) Waychunas, G. A.; Fuller, C. C.; Davis, J. A.; Rehr, J. J. *Geochim. Cosmochim. Acta* **2003**, *67*, 1031.
(4) Bunker, G. *Introduction to XAFS: A Practical Guide to X-ray Absorption Fine Structure Spectroscopy*, 1st ed.; Cambridge University Press: Cambridge, U.K., 2010.
(5) Chan, E. M.; Marcus, M. A.; Fakra, S.; ElNaggar, M.; Mathies, R. A.; Alivisatos, A. P. *J. Phys. Chem. A* **2007**, *111*, 12210.
(6) Ingham, B.; Illy, B. N.; Ryan, M. P. *Curr. Appl. Phys.* **2008**, *8*, 455.

Published on Web 10/28/2010

dilute metal ions in solution make XANES spectroscopy an ideal tool to study CBD of inorganic nanomaterials.

The objective of this work was to determine the time-dependent chemical speciation of Zn(II) during CBD of ZnO nanowires from HMTA and zinc nitrate precursors. Quantifying the speciation of metal ions in aqueous solutions is essential because their speciation strongly affects their reactivity.[7] The growth of ZnO nanowires from HMTA and zinc salt precursors was first observed almost 20 years ago.[8] However, even after numerous studies, the role of HMTA in the reaction and the mechanism of ZnO crystallization remain unclear.[9−16] We have used *in situ* XANES spectroscopy to identify the growth mechanism as direct crystallization and to measure kinetics by quantifying the chemical speciation of Zn(II) during ZnO nanowire growth.

The knowledge of the ZnO nanowire growth chemistry gained from XANES will enable researchers to tailor the morphology and properties of ZnO nanostructures for a wide range of applications. ZnO is a wide band gap semiconductor ($E_g = 3.37$ eV) with a large exciton binding energy (60 meV) that has diverse applications in UV lasers,[17,18] sensors,[19] transparent conducting oxides,[20,21] and nanostructured photovoltaics.[22−27] Recently ZnO nanowire arrays deposited by CBD from zinc nitrate and HMTA precursors have been used for dye sensitized solar cells[24,25,28] and light emitting diodes.[29]

CBD of ZnO nanowires is typically performed at 90 °C with equimolar zinc nitrate and HMTA concentrations in the 10−25 mM range, which produces a pH of ∼5.8. Speciation diagrams[30−32] suggest that $[Zn(H_2O)_6]^{2+}$ is the predominant Zn(II) species at these conditions. However, reliable stability constants for Zn(II)−HMTA complexes do not exist, and extrapolation of other stability constants from room temperature to 90 °C can introduce considerable uncertainty.[33] Therefore, *in situ* spectroscopy to measure the chemical speciation of the metal ion under real reaction conditions is essential to understanding the solution chemistry.

HMTA is a nonionic, heterocyclic organic compound with the formula $(CH_2)_6N_4$. The set of overall reactions most often referenced in the literature[34] for ZnO nanowire deposition from zinc nitrate and HMTA precursors is

$$(CH_2)_6N_4 + 6H_2O \rightarrow 6HCHO + 4NH_3 \quad (1)$$

$$NH_3 + H_2O \leftrightarrow NH_4^+ + OH^- \quad (2)$$

$$2OH^- + Zn^{2+} \leftrightarrow ZnO + H_2O \quad (3)$$

HMTA decomposes upon heating to form formaldehyde and ammonia (eq 1). Ammonia reacts with water to produce OH^- (eq 2), which drives the crystallization of ZnO (eq 3). The crystallization of ZnO could be direct, as illustrated in reaction 3 or could involve an intermediate zinc hydroxide phase.[16]

There have been several, often conflicting, studies over the past decade that investigated the growth of ZnO nanowires from HMTA and various zinc salts. Ashfold found that the HMTA decomposition rate was independent of the ZnO growth rate and concluded that the role of HMTA was only to buffer the pH in solution.[16] Govender concluded that HMTA was not essential to the growth of ZnO nanowires but that it provided a continuous and convenient source of hydroxide.[9] In contrast, Vayssieres proposed that ZnO growth occurred due to the formation and subsequent thermal decomposition of an intermediate Zn(II)−amine complex.[13]

Several studies characterizing hydrates of Zn(II)−HMTA salts with infrared spectroscopy have reported the formation of a Zn(II)−HMTA complex.[35−37] However, conclusions regarding hydrated Zn(II)−HMTA salts are not relevant to an aqueous solution of Zn(II) and HMTA since solvent effects are not present. Tasker and Wood showed that HMTA acts as a strong structure-maker in water, so solvent effects must be considered when evaluating interactions between Zn(II) and HMTA.[38] Thus, understanding the role of HMTA and the speciation of Zn(II) in ZnO growth

(7) Stone, A. T. *Abstr. Pap. Am. Chem. Soc.* **2000**, *220*, 152.
(8) Andres-Verges, M.; Mifsud, A.; Serna, C. J. *J. Chem. Soc., Faraday Trans* **1990**, *86*, 959.
(9) Govender, K.; Boyle, D. S.; Kenway, P. B.; O'Brien, P. *J. Mater. Chem.* **2004**, *14*, 2575.
(10) Greene, L. E.; Law, M.; Tan, D. H.; Montano, M.; Goldberger, J.; Somorjai, G.; Yang, P. D. *Nano Lett.* **2005**, *5*, 1231.
(11) Boercker, J. E.; Schmidt, J. B.; Aydil, E. S. *Cryst. Growth Des.* **2009**, *9*, 2783.
(12) McPeak, K. M.; Baxter, J. B. *Ind. Eng. Chem. Res.* **2009**, *48*, 5954.
(13) Vayssieres, L.; Keis, K.; Lindquist, S. E.; Hagfeldt, A. *J. Phys. Chem. B* **2001**, *105*, 3350.
(14) Vayssieres, L. *Adv. Mater.* **2003**, *15*, 464.
(15) Sugunan, A.; Warad, H. C.; Boman, M.; Dutta, J. *J. Sol-Gel Sci. Technol.* **2006**, *39*, 49.
(16) Ashfold, M. N. R.; Doherty, R. P.; Ndifor-Angwafor, N. G.; Riley, D. J.; Sun, Y. *Thin Solid Films* **2007**, *515*, 8679.
(17) Huang, M. H.; Mao, S.; Feick, H.; Yan, H. Q.; Wu, Y. Y.; Kind, H.; Weber, E.; Russo, R.; Yang, P. D. *Science* **2001**, *292*, 1897.
(18) Bagnall, D. M.; Chen, Y. F.; Zhu, Z.; Yao, T.; Koyama, S.; Shen, M. Y.; Goto, T. *Appl. Phys. Lett.* **1997**, *70*, 2230.
(19) Muller, J.; Weissenrieder, S. *Fresenius J. Anal. Chem.* **1994**, *349*, 380.
(20) Look, D. C. *Mater. Sci. Eng., B* **2001**, *80*, 383.
(21) Tang, W.; Cameron, D. C. *Thin Solid Films* **1994**, *238*, 83.
(22) Baxter, J. B.; Aydil, E. S. *Appl. Phys. Lett.* **2005**, *86*, 053114.
(23) Baxter, J. B.; Aydil, E. S. *Sol. Energy Mater. Sol. Cells* **2006**, *90*, 607.
(24) Baxter, J. B.; Walker, A. M.; van Ommering, K.; Aydil, E. S. *Nanotechnology* **2006**, *17*, S304.
(25) Law, M.; Greene, L. E.; Johnson, J. C.; Saykally, R.; Yang, P. D. *Nat. Mater.* **2005**, *4*, 455.
(26) Leschkies, K. S.; Divakar, R.; Basu, J.; Enache-Pommer, E.; Boercker, J. E.; Carter, C. B.; Kortshagen, U. R.; Norris, D. J.; Aydil, E. S. *Nano Lett.* **2007**, *7*, 1793.
(27) Olson, D. C.; Piris, J.; Collins, R. T.; Shaheen, S. E.; Ginley, D. S. *Thin Solid Films* **2006**, *496*, 26.
(28) Jiang, C. Y.; Sun, X. W.; Tan, K. W.; Lo, G. Q.; Kyaw, A. K. K.; Kwong, D. L. Appl. Phys. Lett. **2008**, *92*.
(29) Lai, E.; Kim, W.; Yang, P. D. *Nano Res.* **2008**, *1*, 123.
(30) Richardson, J. J.; Lange, F. F. *Cryst. Growth Des.* **2009**, *9*, 2570.
(31) Yamabi, S.; Imai, H. *J. Mater. Chem.* **2002**, *12*, 3773.
(32) Peterson, R. B.; Fields, C. L.; Gregg, B. A. *Langmuir* **2004**, *20*, 5114.
(33) Pettit, L.; Pettit, G. *Pure Appl. Chem.* **2009**, *81*, 1585.
(34) Schmidt-Mende, L.; MacManus-Driscoll, J. L. *Mater. Today* **2007**, *10*, 40.
(35) Grodzicki, Z.; Szlky, E. *Polish J. Chem.* **1984**, *58*, 999.
(36) Grodzicki, Z.; Szlky, E. *Polish J. Chem.* **1984**, *58*, 1009.
(37) Chou, K. S.; Chen, W. H.; Huang, C. S. *J. Chin. Inst. Chem. Eng.* **1990**, *21*, 327.
(38) Tasker, I. R.; Wood, R. H. *J. Solution Chem.* **1982**, *11*, 729.

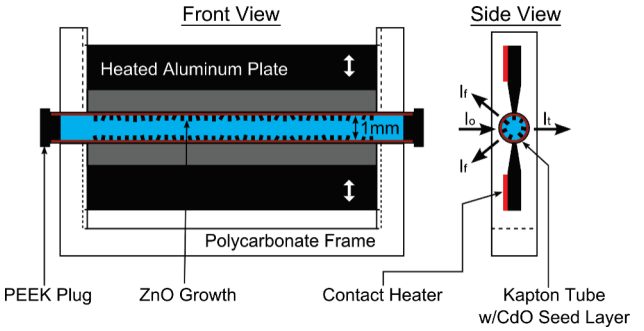

Figure 1. Schematic of microreactor for *in situ* XANES studies. Heated aluminum plates are pressed into contact with the sides of the polyimide tube to control the reactor temperature. A beam of monochromatic X-rays of intensity I_o is incident upon the polyimide tube. The transmitted beam has intensity I_t. X-ray fluorescence, I_f, is collected and analyzed.

chemistry requires *in situ* characterization techniques that are sensitive to the Zn(II) coordination environment. None of the studies mentioned above characterized the ZnO growth reaction *in situ*, with the exception of Ashfold's pH measurements, nor did they use experimental techniques that were highly sensitive to the coordination environment of Zn(II).

Herein we present an analysis of the *in situ* XANES spectra collected from the CBD of ZnO nanowires that shows that only two Zn(II) species are present under normal growth conditions: $[Zn(H_2O)_6]^{2+}$ and ZnO. These results conclusively refute previous theories that ZnO grows via the thermal decomposition of intermediate Zn(II)−HMTA or Zn(II)−ammine complexes or the deprotonation of an intermediate zinc hydroxide. The absence of zinc hydroxide intermediates above the detection limit of ~0.01 mM supports the formation of ZnO by a direct crystallization route. Dynamics of induction, nucleation, and growth phases revealed by time-resolved XANES and the dependence of dynamics on reaction concentration and temperature are also discussed.

Experimental Section

In situ XANES spectra at the Zn K-edge were collected during the aqueous solution growth of ZnO nanowires over a 2 h period. Principal component analysis (PCA) of the time-dependent spectra was used to determine the number of species present during the reaction. The identities of the species were determined by target testing a library of standard XANES spectra against the principal components. The library of standard XANES spectra, described in more detail below, was collected experimentally and consisted of Zn(II) species that have been suggested to be involved in the aqueous solution growth of ZnO nanowires. Finally, the kinetics of the ZnO nanowire growth reaction were calculated by least-squares fitting linear combinations of the appropriate standard XANES spectra to the time-dependent experimental XANES spectra.

Reactor for *In Situ* XANES Spectroscopy. The home-built microreactor used for *in situ* XANES spectroscopy of ZnO nanowire growth is shown schematically in Figure 1. The reaction channel is a polyimide tube (RiverTech Medical) measuring 0.91 mm i.d. × 100 mm long, with a wall thickness of 0.05 mm and a total volume of 65 μL. The inside wall of the polyimide tube was precoated with a sol−gel derived CdO seed layer to enhance the nucleation density of the ZnO deposition. CdO was used instead of ZnO to avoid any Zn X-ray fluorescence (and therefore contamination of the XANES) from the seed layer. To deposit the CdO seed layer, the polyimide tube was oriented vertically and filled by a syringe pump with an ethanol solution containing 0.375 M cadmium acetate and 0.375 M monoethanolamine.[39] The syringe was then withdrawn, leaving a thin layer of the ethanol sol on the inside wall of the tube. Nitrogen was blown through the tube at 5 psi for 1 min to enhance gelation of the ethanol sol layer.[40] The polyimide tube was then annealed in a tube furnace at 400 °C for 20 min.[39] The resulting CdO seed films were polycrystalline with a thickness of ~40 nm and a grain size of ~5−10 nm.

Temperature was maintained to ±0.1 °C in the reaction channel by two heated aluminum plates that were pressed against the outside wall of the polyimide tube. The edges of the aluminum plates in contact with the outside wall of the polyimide tube were tapered to a thickness of 0.25 mm, allowing the microreactor to operate at elevated temperatures without interfering with incident (I_o), fluorescent (I_f), or transmitted (I_t) X-rays (Figure 1). Thermocouples were attached to the tapered edge of the heated aluminum plates and provided feedback to the temperature controller. The set point temperature was reached approximately 12 min after the heaters were activated.

ZnO Nanowire Growth Conditions. ZnO nanowires were deposited on the CdO seed layer at 60 and 90 °C from equimolar aqueous solutions of zinc nitrate and hexamethylenetetramine (HMTA) at concentrations of 4.17, 6.25, and 12.5 mM. At 90 °C, these conditions result in steady-state pH in the range of 5.8−6.2. At high concentrations, ZnO can precipitate in solution in addition to depositing on the CdO seed layer. However, the reaction mechanisms and dominant Zn(II) species identified using XANES will not depend on the nature of the seed layer. The precursor solution was injected into the reaction channel via a syringe. Both ends of the channel were then sealed with polyether ether ketone (PEEK) plugs (Upchurch) to prevent evaporation. Upon completion of each XANES experiment, the polyimide tube was removed from the heating elements, flushed with DI water, and blown dry with nitrogen. *Ex situ* characterization of the deposited material was performed by splitting the polyimide tube longitudinally with a razor blade. These half-tubes were then laid flat onto double sided carbon tape for imaging using scanning electron microscopy (SEM).

Zn(II) XANES Standards. To quantify the speciation of Zn(II), seven species suggested to be involved in ZnO crystallization under different reaction conditions were prepared and used for target testing. These species were ZnO nanopowder (Sigma), ε-$Zn(OH)_2$ (PDF no. 00-038-0385), δ-$Zn(OH)_2$ (PDF no. 00-020-1436), γ-$Zn(OH)_2$ (PDF no. 00-020-1437), 12.5 mM $[Zn(H_2O)_6]^{2+}$, 12.5 mM $[Zn(NH_3)_4]^{2+}$, and 12.5 mM $[Zn(OH)_4]^{2-}$. XANES spectra from solid phase standards were recorded at 25 °C, and spectra from aqueous standards were recorded at 60 and 90 °C. ε and δ phases of $Zn(OH)_2$ were synthesized using methods outlined by Ping et al.[41] and Shaporev et al.,[42] respectively. Details of the synthesis for all the $Zn(OH)_2$ phases and X-ray diffraction of the powders are provided in the Supporting Information. Zinc nitrate

(39) Ghosh, P. K.; Das, S.; Chattopadhyay, K. K. *J. Nanopart. Res.* **2005**, *7*, 219.
(40) Jing, C. B.; Zhao, X. J.; Han, J. J.; Zhu, K.; Liu, A. Y.; Tao, H. Z. *Surf. Coat. Technol.* **2003**, *162*, 228.
(41) Ping, L. I.; Ping, Z.; Bin, L.; Zhen-bin, J.; Yu, W. *Chem. Res. Appl.* **2004**, 16.
(42) Shaporev, A. S.; Ivanov, V. K.; Baranchikov, A. E.; Polezhaeva, O. S.; Yu, D. T. y. *Russ. J. Inorg. Chem.* **2007**, *52*, 1811.

hexahydrate (Sigma) was used as the Zn(II) source for the $Zn(OH)_2$ phases as well as the Zn(II) aqueous complexes.

The selection of pH and ammonium concentration necessary to isolate the $[Zn(NH_3)_4]^{2+}$ and $[Zn(OH)_4]^{2-}$ complexes was guided by the use of Zn(II) speciation diagrams.[30−32] The $[Zn(NH_3)_4]^{2+}$ complex was synthesized using 12.5 mM $Zn(NO_3)_2$ and 0.375 M NH_4NO_3. The pH was adjusted with the addition of 0.3 M NaOH to 8.9 and 8.2 at 60 and 90 °C, respectively. The $[Zn(OH)_4]^{2-}$ complex was prepared using 12.5 mM $Zn(NO_3)_2$. The pH was adjusted by the addition of 0.45 M NaOH to 12 and 11.5 at 60 and 90 °C, respectively. The pH of the 12.5 mM $[Zn(H_2O)_6]^{2+}$ solution was 5.1 and 4.7 at 60 and 90 °C, respectively. The pH of the solution was not adjusted since the pK_a for $[Zn(H_2O)_6]^{2+}$ at 25 °C is 8.96.[43,44] All pH measurements were acquired with an Orion 4-star pH meter with a ROSS Ultra electrode. The pH meter was calibrated at the measured solution temperature with fresh buffer solutions at pH 4, 7, and 10. All solution phase standards were injected into bare polyimide tubes, except the $[Zn(OH)_4]^{2-}$ complex, where a PTFE-lined polyimide tube (MicroLumen) was used to avoid dissolution of the polyimide by the alkaline solution.

Beamline Conditions for XANES. Zn K-edge XANES experiments were performed at the Insertion Device (ID) beamline of the Materials Research Collaborative Access Team (MRCAT) line at the Advanced Photon Source, Argonne National Laboratory. The first harmonic of the undulator was used, and the undulator was tapered to reduce the variation in the intensity of the incident X-ray beam to about 30% over the energy region scanned. Linearity tests of the microreactor setup with a 12.5 mM $[Zn(H_2O)_6]^{2+}$ solution showed less than 0.1% nonlinearity for a 50% decrease in incident beam intensity. The incident beam area was defined as 0.5 mm by 0.5 mm. A cryogenically cooled Si (111) double crystal monochromator was used for energy selection. A Rh-coated mirror positioned after the monochromator was used at grazing incidence to minimize higher harmonics produced by the undulator and passed by the monochromator. The incident beam intensity was measured using an ion chamber with a mixture of 80% He and 20% N_2. The X-ray fluorescence intensity (I_f) was measured using a 5-grid Lytle detector filled with Ar. For energy calibration, a Zn foil reference spectrum was measured with each scan. The monochromator was scanned in 0.5 eV steps with an integration time of 0.075 s. The resulting scan length of 93 s is considerably faster than the reaction dynamics we are measuring.

Radiation did not induce measurable changes in the ZnO over the time scale of the experiment. A series of spectra of ZnO nanowires were acquired after the reaction channel was flushed with DI water and blown dry with N_2. Scans showed less than 0.4% change in the whiteline over 2 h, with no trend in the variations over time. Details of the radiation damage tests can be found in the Supporting Information.

Note that the X-rays from the undulator are polarized in the horizontal direction. With the particular sample geometry we were using, we are largely probing structure perpendicular to the nanowire growth direction. For the results presented in this study, however, this should have a very small effect.

XANES Data Analysis. Standard XAFS data analysis procedures were followed. Normalization and linear combination fitting of standard spectra to the time-dependent experimental spectra were performed using Athena.[45] SixPACK[46] was used for PCA and target testing of the normalized spectra.

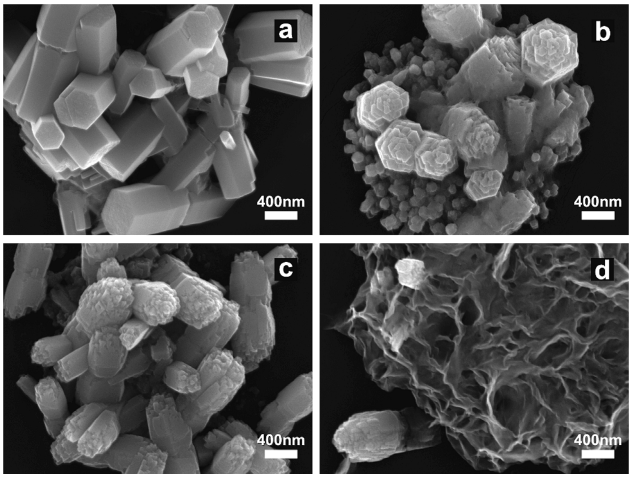

Figure 2. SEM images of ZnO after 2 h of growth on the CdO-seeded polyimide tube at various reaction conditions: (a) 12.5 mM $Zn(NO_3)_2$/HMTA at 90 °C, (b) 6.25 mM $Zn(NO_3)_2$/HMTA at 90 °C, (c) 4.17 mM $Zn(NO_3)_2$/HMTA at 90 °C, and (d) 12.5 mM $Zn(NO_3)_2$/HMTA at 60 °C. Electron diffraction confirms that each of the structures is wurtzite ZnO.

***Ex Situ* Characterization.** Deposited ZnO was characterized *ex situ* by scanning electron microscopy (SEM, Zeiss Supra 50VP) and transmission electron microscopy (TEM, JEOL JEM2100). The crystalline phase of all solid XANES standards was verified by X-ray diffraction (XRD, Rigaku SmartLab) with Cu Kα radiation. Each sample contained only the pure specified phase with no detectable secondary phases.

Results and Discussion

Synthesis and *Ex Situ* Characterization of Deposited ZnO. ZnO nanowires grown at 90 °C are well-faceted with hexagonal cross sections and diameters of 300−500 nm. In general, nanowires grown from a CdO seed layer are less densely packed and less vertically oriented than those grown from a homoepitaxial (0002) ZnO seed layer.[10,12,14,47] CdO is insoluble in aqueous solutions and does not interfere in the growth reactions.

The micrographs in Figure 2 show ZnO nanowires deposited at 90 °C from 12.5, 6.25, and 4.17 mM concentrations after 2 h, as well as growth at 60 °C with 12.5 mM concentration. Deposited material in Figure 2a−c has a hexagonal structure indicative of wurtzite ZnO, which was confirmed by transmission electron microscopy (TEM). At 60 °C, two distinct growth morphologies were present: hemispherical honeycomb-like structures and poorly faceted nanowires. The majority of nanowires appear to grow from the hemispherical honeycomb-like structures, rather than directly from the CdO seed layer as they do at 90 °C. TEM electron diffraction confirmed that the honeycomb-like structures are crystalline ZnO. An electron diffraction pattern of the honeycomb structure is provided in the Supporting Information.

ZnO can also precipitate through homogeneous nucleation and growth in solution. However, diffusion

(43) Miyanaga, T.; Watanabe, I.; Ikeda, S.; Tashiro, K.; Fujikawa, T. *Bull. Chem. Soc. Jpn.* **1988**, *61*, 3199.
(44) Cauët, E.; Bogatko, S.; J. H., W.; Fulton, J. L.; Schenter, G. K.; Bylaska, E. J. *J. Chem. Phys.* **2010**, *132*, 13.
(45) Ravel, B.; Newville, M. *J. Synchrotron Radiat.* **2005**, *12*, 537.
(46) Webb, S. M. *Phys. Scr.* **2005**, *T115*, 1011.
(47) Lee, Y. J.; Sounart, T. L.; Scrymgeour, D. A.; Voigt, J. A.; Hsu, J. W. P. *J. Cryst. Growth* **2007**, *304*, 80.

lengths to the seeded reactor walls are very short due to the submillimeter tube diameters. Therefore, most ZnO growth occurs from the CdO seed film because of the reduced energy barrier for heterogeneous nucleation compared to homogeneous nucleation. Visual inspection showed small amounts of precipitation, with less precipitation at lower concentrations and temperatures. The mechanisms of ZnO growth elaborated upon later will not depend on the identity of the seed.

***In Situ* XANES Spectroscopy of Zn(II).** *In situ* spectroscopic monitoring of chemical speciation during crystallization from solution is a great challenge. In CBD, very little characterization of the ions in solution, beyond pH, is typically performed. This is primarily due to the dilute nature of the solutions, which makes Raman and infrared spectroscopy difficult,[48] and the lack of long-range order that is required by X-ray diffraction. X-ray and electron diffraction can be used to characterize the deposited crystalline material, but they give no information about the coordination environment of the metal ion in the liquid phase.

XANES spectroscopy is an ideal technique to study crystallization from solution because it is an element-specific probe that is highly sensitive to the local structure around the absorbing atom. This high degree of sensitivity to the coordination environment of the absorber atom is due to the perturbation of the wave function of the ejected photoelectron by multiple scattering events from the surrounding atoms.[3] The structural sensitivity of XANES spectroscopy allows the chemical speciation of metal ions to be determined, assuming that the proper standards can be obtained or synthesized. XANES works equally well for noncrystalline and crystalline materials and is sensitive to low concentrations of absorber atoms.[49] Furthermore, short XANES scan times enable time-resolved studies of dynamics on scales of minutes to hours.[50,51]

Time-dependent Zn K-edge XANES spectra of ZnO nanowire growth from equimolar 12.5 mM zinc nitrate/HMTA precursors at 90 and 60 °C are shown in Figure 3. Time begins when the heater is turned on. The reactor reaches the set point temperature in ~12 min. XANES spectra acquired at 90 °C change rapidly during the initial ~30 min due to the nucleation of ZnO, then change gradually for the remaining reaction time during the ZnO growth phase. The transition from disordered, noncrystalline material to ordered, crystalline material is marked by an increasingly sharp energy-dependent structure in the normalized absorption coefficient with increasing reaction time. Time-dependent XANES spectra of ZnO nanowire growth from 6.25 and 4.17 mM zinc nitrate/HMTA at 90 °C (not shown) appeared very

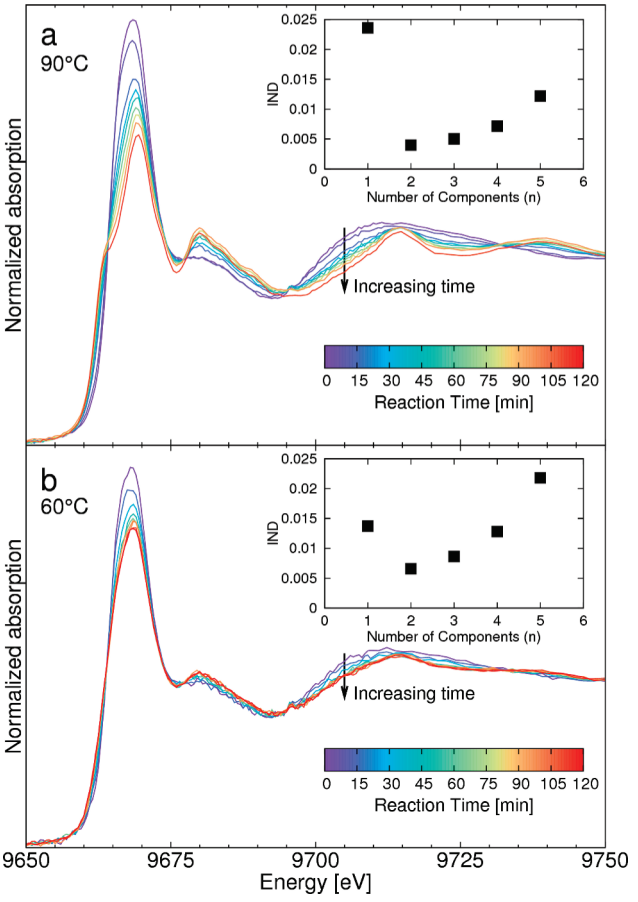

Figure 3. *In situ*, time-resolved Zn K-edge XANES spectra of ZnO nanowire growth at (a) 90 °C and (b) 60 °C over a period of 2 h. Insets show the indicator (IND) function, which has its minimum at two components for both 90 and 60 °C growth temperatures.

similar to growth from the 12.5 mM zinc nitrate/HMTA bath. Changes in the XANES spectra are smaller in magnitude when the microreactor is operated at 60 °C than at 90 °C, but they follow a qualitatively similar pattern. The smaller changes in the XANES spectra acquired at lower temperature over the same time period are due to slower formation of ZnO. The rate-limiting step in ZnO formation is the thermal decomposition of HMTA to hydroxide ions, which has slower kinetics at lower temperatures.[52]

Quantitative Analysis of XANES Data to Identify Principal Zn(II) Species. Qualitative analysis of time-dependent XANES spectra can provide insight into relative reaction rates and the transition from disordered to ordered material, but determining the number and identity of the species involved in the ZnO nanowire growth requires quantitative analysis of the spectra. Principal component analysis (PCA) was used to determine the number of components present in an experimental data set.[53] PCA is widely used in the chemometrics field and has been successfully applied to determine the number of

(48) Bockris, J. O. M.; Reddy, A. K. N. *Modern Electrochemistry: Ionics*; Plenum Press: New York, 1998.
(49) Ressler, T.; Wong, J.; Roos, J.; Smith, I. L. *Environ. Sci. Technol.* **2000**, *34*, 950.
(50) Smolentsev, G.; Guilera, G.; Tromp, M.; Pascarelli, S.; Soldatov, A. V. J. Chem. Phys. **2009**, *130*.
(51) Brendt, J.; Samuelis, D.; Weirich, T. E.; Martin, M. *Phys. Chem. Chem. Phys.* **2009**, *11*, 3127.
(52) Jolivet, J. P. *Metal Oxide Chemistry and Synthesis: From Solution to Solid State*; John Wiley & Sons Ltd.: West Sussex, England, 2000.
(53) Malinowski, E. R. *Factor Analysis in Chemistry*; 3rd ed.; Wiley: New York, 2002.

chemical species in several previous time-resolved and equilibrium XANES studies.[49,54,55] A detailed explanation of the single value decomposition (SVD) algorithm used in the PCA for this work can be found in Ressler et al.[49] Once the SVD algorithm has been applied to a data set, several statistical criteria such as the indicator function (IND),[56] the imbedded error function,[56] and F-tests[54] can be used to determine the number of principal components in the data set. The IND function, which reaches a minimum at the number of principal components in the system, was used for this work due to its robustness and previous success in XANES studies.[46,54] The IND function is an empirical function developed by Malinowski that relies on the secondary eigenvalues from the PCA.[56]

Two principal components are required to minimize the IND function for XANES spectra in this work, as shown in the insets of Figure 3. The IND function indicates that exactly two Zn(II) species are present in ZnO nanowire growth from equimolar 12.5 mM zinc nitrate/HMTA at both 90 and 60 °C. If intermediate species existed, slower reaction kinetics at 60 °C could increase their steady state concentration. However, the lack of a third component at either temperature supports the theory that ZnO crystallizes directly, without the presence of long-lived intermediates.

Target testing identified the two principal components indicated by PCA to be $[Zn(H_2O)_6]^{2+}$ and ZnO. Target testing, also referred to as target transformation, is a powerful technique which allows the chemical composition of an unknown species in a mixture to be determined without any *a priori* knowledge of the species.[54] On the basis of the IND function, target transformations were performed using the two components from the PCA data set to identify the two Zn(II) species. Figures 4 and 5 show seven standard XANES spectra and the calculated two-component target transforms for growth at 90 and 60 °C, respectively. The XANES standards chosen were solid ZnO, ε-$Zn(OH)_2$, δ-$Zn(OH)_2$, and γ-$Zn(OH)_2$ and 12.5 mM aqueous $[Zn(H_2O)_6]^{2+}$, $[Zn(NH_3)_4]^{2+}$, and $[Zn(OH)_4]^{2-}$. These seven standards are the dominant species over a wide range of temperature and pH conditions potentially useful for ZnO synthesis. For both 90 and 60 °C, the transforms provide excellent fits to the $[Zn(H_2O)_6]^{2+}$ and ZnO standards. However, the other five standards clearly cannot be fit with linear combinations of the two principal components, and we conclude that they are not present in significant concentrations at any point during the reaction. For completeness, target transforms were also calculated with three principal components (not shown). Again, the three-component transforms calculated at both 90 and 60 °C provided excellent fits to the $[Zn(H_2O)_6]^{2+}$ and ZnO standards but not to the other standards.

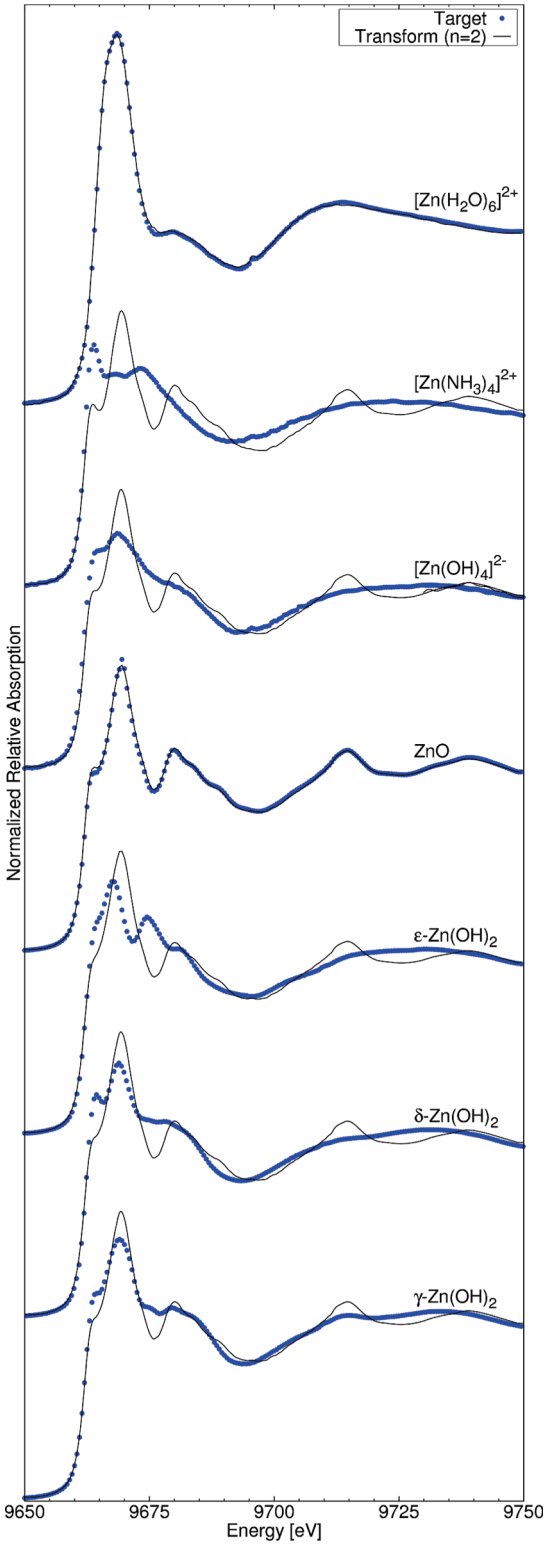

Figure 4. XANES spectra of Zn(II) standards for seven species potentially present in ZnO crystallization (blue dots) compared to target transforms using the two principal components calculated from the time-dependent XANES data set obtained at 90 °C (black line). Only target transforms to the $[Zn(H_2O)_6]^{2+}$ and ZnO standards provide suitable fits. Therefore, none of the other standards are present in measurable quantities (> 0.01 mM) during the reaction.

The standard XANES spectra for the zinc hydroxide phases and the Zn(II)−ammine complexes are distinctly different than the XANES spectra for $[Zn(H_2O)_6]^{2+}$ and

(54) Beauchemin, S.; Hesterberg, D.; Beauchemin, M. *Soil Sci. Soc. Am. J.* **2002**, *66*, 83.
(55) Ressler, T.; Timpe, O.; Neisius, T.; Find, J.; Mestl, G.; Dieterle, M.; Schlogl, R. *J. Catal.* **2000**, *191*, 75.
(56) Malinowski, E. R. *Anal. Chem.* **1977**, *49*, 612.

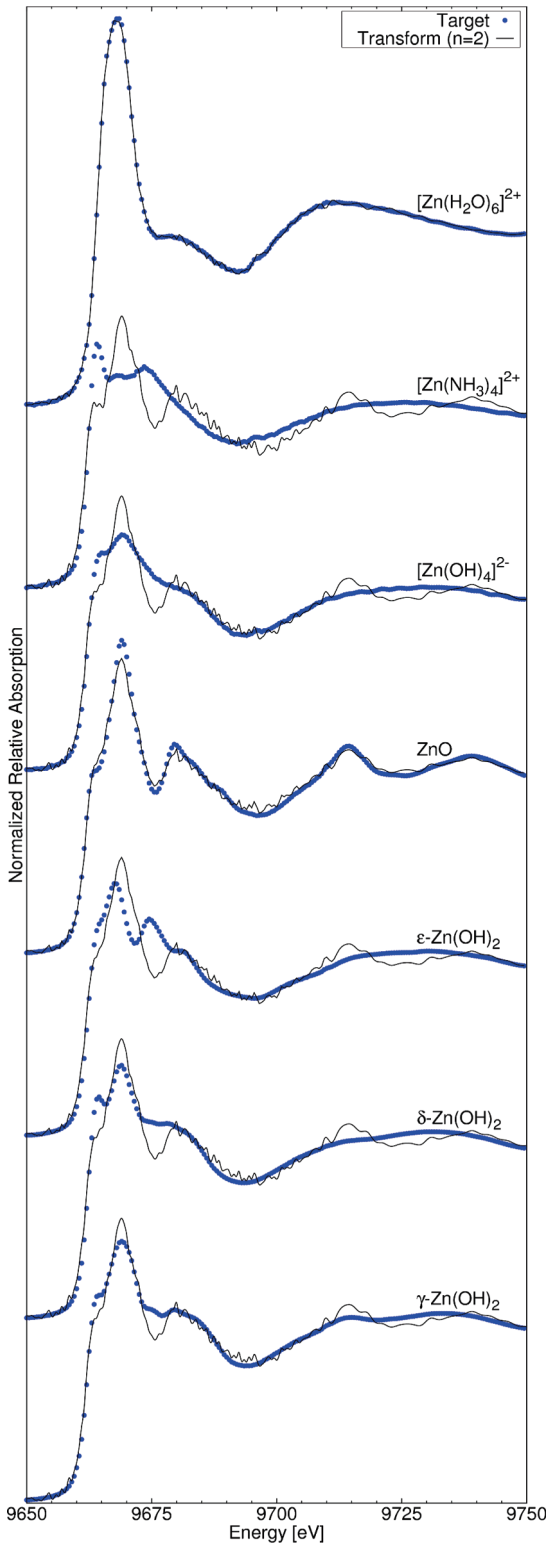

Figure 5. XANES spectra of Zn(II) standards for same seven species as Figure 4 (blue dots) compared to target transforms using the two principal components calculated from the time-dependent XANES data set obtained at 60 °C (black line). Only target transforms to the $[Zn(H_2O)_6]^{2+}$ and ZnO standards provide suitable fits. Therefore, none of the other standards are present in measurable quantities (> 0.01 mM) during the reaction even at low temperatures that may increase the lifetime of intermediates.

ZnO and cannot be fit by two- or even three-component target transformations. Therefore, concentrations of zinc hydroxide or Zn(II)−ammine must be below the sensitivity level of this work (~0.01 mM). Their presence in measurable quantities would skew the time-dependent XANES spectra and change the position of the IND minimum. The presence of an intermediate Zn(II)−HMTA complex is also unlikely. HMTA has been reported to be a bidentate ligand, bridging between two transition metal ions.[57] Water, hydroxide, and ammine are all monodentate ligands with Zn(II).[58] The bidentate nature of the HMTA ligand would change the coordination environment of Zn(II) and thus alter the XANES spectra significantly. In summary, target testing shows that ZnO growth from aqueous $Zn(NO_3)_2$ and HMTA precursors occurs via direct crystallization, without the presence of zinc hydroxide, Zn(II)−ammine, or Zn(II)−HMTA intermediates.

Measuring Dynamics Using Time-Resolved XANES. Dynamics of ZnO growth were studied by fitting linear combinations of the $[Zn(H_2O)_6]^{2+}$ and ZnO standard spectra to the time-dependent XANES spectra. Figure 6 shows the change in $[Zn(H_2O)_6]^{2+}$ and ZnO fractions as a function of time for several equimolar $Zn(NO_3)_2$ and HMTA concentrations and growth temperatures. Linear combinations of the standard spectra were not forced to sum to one. Results from ZnO growth at 90 °C (Figure 6a−c) all display a similar pattern. No ZnO grows during the initial ~8 min induction period that occurs during heating. Induction is followed by rapid ZnO nucleation and growth for ~10 min. ZnO growth then proceeds linearly and eventually slows and terminates as the ZnO saturation index approaches zero. This growth pattern has been observed in previous studies of chemical bath deposition.[1,12] However, the ability to resolve both chemical speciation and kinetic information simultaneously is unique to this work.

The fraction of $[Zn(H_2O)_6]^{2+}$ converted to ZnO during the nucleation phase increases as the initial concentration of $Zn(NO_3)_2$ decreases, as shown in Figure 6a−c. The number of nucleation sites available on the CdO seed layer is sufficiently high that at lower initial concentrations most of the $[Zn(H_2O)_6]^{2+}$ species are converted to ZnO during the nucleation phase. However, at high initial concentration, a significant amount of $[Zn(H_2O)_6]^{2+}$ remains in solution after nucleation and an extended linear growth regime can proceed.

During the nucleation phase, the growth rate of ZnO is independent of the initial $[Zn(H_2O)_6]^{2+}$ and HMTA concentration. The inset of Figure 6a shows a plot of ZnO concentration (fraction of ZnO multiplied by the initial concentration of $[Zn(H_2O)_6]^{2+}$) versus time for 90 °C growth at 4.17, 6.25, and 12.5 mM concentrations. The three ZnO growth curves overlay at early times for all initial $[Zn(H_2O)_6]^{2+}$/HMTA concentrations, illustrating that ZnO growth rate during the nucleation phase is independent of concentration. Instead, the number of available CdO surface sites limits the growth rate of ZnO during the nucleation phase. After the nucleation period, ZnO growth proceeds

(57) Ahuja, I. S.; Yadava, C. L.; Singh, R. *J. Mol. Struct.* **1982**, *81*, 229.
(58) Cotton, F. A.; Wilkinson, G.; Murillo, C. A. *Advanced Inorganic Chemistry*; Wiley: New York, 1999.

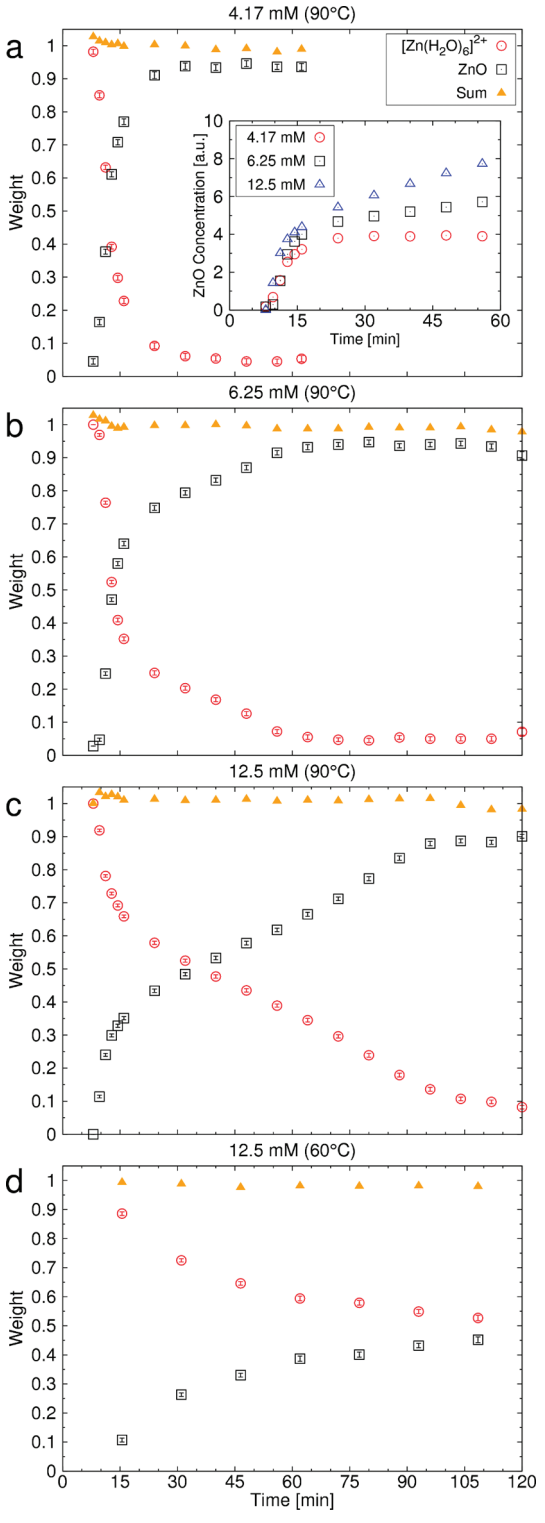

Figure 6. Linear combination fits of $[Zn(H_2O)_6]^{2+}$ (open squares) and ZnO (open circles) standard XANES spectra to the time-resolved experimental data sets. Dynamics are shown for the following equimolar concentrations of $Zn(NO_3)_2$ and HMTA and growth temperatures: (a) 4.17 mM and 90 °C, (b) 6.25 mM and 90 °C, (c) 12.5 mM and 90 °C, and (d) 12.5 mM and 60 °C. "Weight" refers to the fraction of each standard spectrum used to fit the XANES data and does not translate directly to physical weight fraction. Summation of weights of 12.5 mM $[Zn(H_2O)_6]^{2+}$ and ZnO standard spectra are plotted as triangles. Weights were not forced to sum to one. Inset shows concentration of ZnO (ZnO weight multiplied by initial concentration of $[Zn(H_2O)_6]^{2+}$) versus time at 4.17, 6.25, and 12.5 mM $[Zn(H_2O)_6]^{2+}$ concentrations at 90 °C growth. ZnO growth rate is independent of concentration during the nucleation phase.

linearly with faster linear growth rates in cases which had larger initial, and hence larger remaining, $[Zn(H_2O)_6]^{2+}$/HMTA concentrations.

Figure 6d shows linear combination fits of ZnO growth from an equimolar 12.5 mM $Zn(NO_3)_2$/HMTA solution at 60 °C. The overall reaction kinetics at 60 °C are slower by approximately a factor of 4 than kinetics at 90 °C (Figure 6c). Furthermore, the nonlinear growth regime, indicative of nucleation, is ~15 min longer. The slower kinetics at 60 °C are most likely due to a reduced rate of thermal decomposition of HMTA to hydroxide ions.[12,52]

The fraction of $[Zn(H_2O)_6]^{2+}$ and ZnO species for all concentrations and growth temperatures sums to one (Figure 6, triangles), within the experimental error. The increased discrepancy for the summations at times less than 12 min arises because the reactor had not yet reached the set-point temperature. The XANES spectra of $[Zn(H_2O)_6]^{2+}$ has a small temperature dependence because the intensity of the white line is suppressed at higher temperatures due to fewer excited states being available to the photoelectron. Therefore, the $[Zn(H_2O)_6]^{2+}$ standard acquired at 60 or 90 °C does not fit quite as well to the experimental spectra acquired at lower temperatures. The summation of the fractions of $[Zn(H_2O)_6]^{2+}$ and ZnO to one, without constraining the fitting procedure, further verifies that ZnO growth occurs by direct crystallization without long-lasting intermediates.

Conclusions

We have demonstrated the first *in situ* X-ray absorption study of the chemical bath deposition (CBD) of nanostructures. The sensitivity of XANES spectroscopy to the coordination environment of the absorber element, its low detection limit, and its ability to characterize liquid, amorphous, and crystalline materials make it an excellent tool for *in situ* characterization of metal ion speciation during CBD. Furthermore, the use of principal component analysis, target testing, and linear combination fitting of standard spectra can be used to elucidate reaction pathways and kinetics. Improved fundamental understanding of CBD reactions will aid in tailoring the reaction conditions for current chemistries to improve the properties of the deposited materials and could also enable novel synthesis routes for new materials.

We have applied *in situ* XANES spectroscopy to zinc nitrate/HMTA chemistry to show that ZnO crystallizes directly from $[Zn(H_2O)_6]^{2+}$ without any long-lived intermediates. HMTA does not act as a metal-ion buffer in the CBD of ZnO nanowires. Instead, the thermal decomposition of HMTA provides a controlled source of hydroxide ions for the crystallization of ZnO. The slow release of hydroxide ions minimizes the nonequilibrium saturation index of ZnO in solution. Controlling pH in this manner promotes heterogeneous growth over homogeneous nucleation by avoiding a high ZnO saturation index. Understanding the role of HMTA and the dependence of reaction kinetics on concentration and

temperature will enable optimization of reaction conditions to synthesize ZnO nanowire arrays for applications such as photovoltaics, optoelectronics, and sensors.

Acknowledgment. MRCAT operations are supported by the Department of Energy and the MRCAT member institutions. J.B. acknowledges support from NSF through Awards CAREER CBET-0846464 and CMMI-1000111. The authors are grateful to Drexel University's Centralized Research Facility for their instrumentation support.

Supporting Information Available: Details on the synthesis of the different zinc hydroxide phases with X-ray diffraction scans of the powders, TEM of deposition at 60 °C, and ZnO radiation damage tests (PDF). This material is available free of charge via the Internet at http://pubs.acs.org.